Sierpiński fractal plasmonic antenna: a fractal abstraction of the plasmonic bowtie antenna

Shawn Sederberg and A.Y. Elezzabi

Department of Electrical and Computer Engineering, University of Alberta, Edmonton, Alberta T6G 2V4, Canada
elezzabi@ece.ualberta.ca

Abstract: A new class of bowtie antennas with Sierpiński fractal features is proposed for sensing molecular vibration modes in the near- to mid-infrared. These antennas offer a compact device footprint and an enhanced confinement factor compared to a bowtie antenna. Through extensive simulations, it is shown that these characteristics are related to the ability of this fractal geometry to become polarized. Simulation results demonstrate that these antennas may be tuned between 700nm ≤ λ ≤ 3.4μm and that electric field enhancement by 56 is possible at the center of the antenna gap.

OCIS codes: (250.5403) Plasmonics; (350.4238) Nanophotonics and photonic crystals; (260.3910) Metal optics; (310.6628) Subwavelength structures, nanostructures; (140.4780) Optical resonators; (260.5740) Resonance.

References and links

1. B. B. Mandelbrot, *The Fractal Geometry of Nature* (W.H. Freeman, 1982).
2. K. J. Falconer, *Fractal Geometry: Mathematical Foundations and Applications* (Wiley, 2003).
3. D. H. Werner, and S. Ganguly, "An overview of fractal antenna engineering research," IEEE Trans. Antennas Propag. **45**, 38–57 (2003).
4. C. Gaubert, L. Chusseau, A. Giani, D. Gasquet, F. Garet, F. Aquistapace, L. Duvillaret, J.-L. Coutaz, and W. Knap, "THz fractal antennas for electrical and optical semiconductor emitters and receptors," Phys. Status Solidi **1**(6 c), 1439–1444 (2004).
5. Y.-J. Bao, B. Zhang, Z. Wu, J.-W. Si, M. Wang, R.-W. Peng, X. Lu, J. Shao, Z.-F. Li, X.-P. Hao, and N.-B. Ming, "Surface-plasmon-enhanced transmission through metallic film perforated with fractal-featured aperture array," Appl. Phys. Lett. **90**(25), 251914 (2007).
6. F. Miyamaru, Y. Saito, M. W. Takeda, B. Hou, L. Liu, W. Wen, and P. Sheng, "Teraherz electric response of fractal metamaterial structures," Phys. Rev. B **77**(4), 045124 (2008).
7. A. Agrawal, T. Matsui, W. Zhu, A. Nahata, and Z. V. Vardeny, "Terahertz spectroscopy of plasmonic fractals," Phys. Rev. Lett. **102**(11), 113901 (2009).
8. J. Matteo, and L. Hesselink, "Fractal extensions of near-field aperture shapes for enhanced transmission and resolution," Opt. Express **13**(2), 636–647 (2005).
9. B. Hou, X. Q. Liao, and J. K. S. Poon, "Resonant infrared transmission and effective medium response of subwavelength H-fractal apertures," Opt. Express **18**(4), 3946–3951 (2010).
10. L. Novotny, "Effective wavelength scaling for optical antennas," Phys. Rev. Lett. **98**(26), 266802 (2007).
11. A. Alù, and N. Engheta, "Input impedance, nanocircuit loading, and radiation tuning of optical nanoantennas," Phys. Rev. Lett. **101**(4), 043901 (2008).
12. G. W. Hanson, "On the applicability of the surface impedance integral equation for optical and near infrared copper dipole antennas," IEEE Trans. Antenn. Propag. **54**(12), 3677–3685 (2006).
13. A. Alù, and N. Engheta, "Tuning the scattering response of optical nanoantennas with nanocircuit loads," Nat. Photonics **2**(5), 307–310 (2008).
14. J. S. Huang, T. Feichtner, P. Biagioni, and B. Hecht, "Impedance matching and emission properties of nanoantennas in an optical nanocircuit," Nano Lett. **9**(5), 1897–1902 (2009).
15. S. A. Maier, *Plasmonics: Fundamentals and Applications* (Springer, 2007).
16. L. Wang, and X. Xu, "High transmission nanoscale bowtie-shaped aperture probe for near-field optical imaging," Appl. Phys. Lett. **90**(26), 261105 (2007).
17. S. Kim, J. Jin, Y.-J. Kim, I.-Y. Park, Y. Kim, and S.-W. Kim, "High-harmonic generation by resonant plasmon field enhancement," Nature **453**(7196), 757–760 (2008).
18. P. B. Johnson, and R. W. Christy, "Optical constants of the noble metals," Phys. Rev. B **6**(12), 4370–4379 (1972).

#143637 - $15.00 USD Received 14 Mar 2011; revised 28 Mar 2011; accepted 29 Mar 2011; published 12 May 2011

19. A. Vial, A.-S. Grimault, D. Macias, D. Barchiesi, and M. L. de la Chapelle, "Improved analytical fit of gold dispersion: Application to the modeling of extinction spectra with a finite-difference time-domain method," Phys. Rev. B **71**(8), 085416 (2005).
20. D. P. Fromm, A. Sundaramurthy, P. J. Schuck, G. Kino, and W. E. Moerner, ""Gap-Dependent Optical Coupling of Single "Bowtie" Nanoantennas Resonant in the Visible," Nano Lett. **4**(5), 957–961 (2004).

1. Introduction

Despite the prominent role that Euclidean geometry plays in mathematics, science, and engineering, there are very few objects in nature that it accurately describes. Many naturally-occurring structures are composed of features with numerous length scales, where each length scale appears similar to the others when magnified by an appropriate factor. Common examples include a snowflake, a tree and a coastline. A mathematical abstraction of Euclidean geometry which acts as a much better descriptor of these self-similar or self-affine objects is fractal geometry [1]. Rather than being described by elementary shapes such as polygons and arcs, a fractal is defined by a basis shape and an operator that acts iteratively on that shape. Applying the operator to the basis shape produces the first-iteration shape; applying it again to the first-iteration shape produces the second-iteration shape; and so on. When carried out an infinite number of times, the resulting shape may exhibit interesting properties, such as zero area and infinite perimeter simultaneously. Notably, fractals exist in a space that is characterized by a non-integer, or fractional, dimension [2].

In electromagnetic theory, the manner in which an object scatters an incident photon is strongly dependent on the size of that object relative to the wavelength spectrum that composes the photon. The presence of numerous length scales in fractal structures makes their interaction with electromagnetic radiation intriguing and suggests that the object may act preferentially in multiple bands of wavelengths. Furthermore, a fractal may have a much larger perimeter-to-footprint ratio than its basis shape, leading to red-shifted resonance conditions and compact devices. Numerous microwave antenna designs incorporating fractal geometry have been investigated both theoretically and experimentally and appealing properties including a compact footprint and multiband operation have been successfully demonstrated [3]. Fractal antennas and apertures have also been investigated at terahertz frequencies with similar results [4–7]. It has been demonstrated that nanoscale fractal apertures allow for enhanced transmission and resolution for near- to mid-infrared wavelengths, but multiband behavior is less pronounced at this spectral range [8,9].

In contrast to the vast development of microwave antennas, research in optical antennas is relatively at its infancy. This is largely because the fabrication and characterization technologies that are necessary for these nanometer length scale structures have only recently become accessible. Furthermore, the sophisticated design techniques that have lead to the development of microwave circuits do not directly apply to the optical regime [10–12]. In relatively new theoretical developments, a more systematic approach to designing optical antennas and circuits has been formalized [13,14]. In the optical regime, the behavior of noble metals deviates acutely from that of a perfect electric conductor and can be better described by a strongly-coupled plasma model. Most notably, there exists a size-dependant plasmon resonance condition at which the nanostructure becomes strongly polarized [15]. For a well-designed noble metal antenna, the antenna geometry along with the plasmon resonance can enhance the electric field by more than two orders of magnitude in the antenna gap.

Optical antennas and apertures have been used to enhance near-field scanning optical microscopy (NSOM) probe performance [16] and to increase the efficiency of sensitive physical processes such as high-harmonic generation in argon gas [17]. The nanoscale antenna dimensions combined with the large electric field enhancement in the antenna gap enabled an extremely small array device footprint of approximately $100\mu m^2$, making it compact enough to integrate onto a chip. Furthermore, the authors were able to observe the 17th harmonic using only a standard Ti:Sapphire laser, something that has previously required chirped pulse amplification. This demonstrates that optical antennas are a powerful tool and enable

#143637 - $15.00 USD Received 14 Mar 2011; revised 28 Mar 2011; accepted 29 Mar 2011; published 12 May 2011

relatively easy access to very complex physical processes. Challenges arise when the experimenter wishes to observe a process in the near- or mid-infrared, such as molecular vibration modes, and antenna dimensions must be increased. For example, shifting the resonance from 800nm to 2.5μm increases the device footprint by an order of magnitude, hindering integration onto a chip. In the interest of harnessing light for efficient nanometer-resolution vibrational spectroscopy of molecules in the near- and mid-infrared, it would be advantageous to develop antennas to operate in mid-infrared spectral range, yet maintain a nanoscale footprint and imaging resolution. The development of such an antenna would open a new domain in plasmonics and sensing.

2. The Sierpiński fractal plasmonic antenna

An antenna design that has undergone intensive research at optical and near-infrared wavelengths is the bowtie antenna, which is composed of two triangles. The Sierpiński triangle is a class of fractal that uses triangles as a basis shape. Placing two Sierpiński triangles together forms a modified bowtie antenna which will be referred to as the Sierpiński Fractal Plasmonic Antenna (SFPA). In the first iteration of this structure, each of the two triangles in the bowtie antenna configuration is divided into four equal-sized triangles and the triangle in the center is excluded from the shape, as shown in Fig. 1(a)-(b). In subsequent iterations, the same operation is applied to each of the new triangles that compose the overall structure, as shown in Fig. 1(c)-(d). At each iteration, the number of triangles increases by a factor of three and the length scale of each of these triangles decreases by a factor of two. A quantitative property that summarizes these dynamics of the Sierpiński triangle is the Hausdorff dimension [2]. This is defined as:

$$D = \frac{\log(N)}{\log(S)},$$

where N is the factor by which the number of triangles increases after each iteration, and S is the length scaling factor by which the triangles are reduced. The Hausdorff dimension is a measure of the extent to which a fractal occupies space.

The ability of an ensemble of triangles to become polarized depends on the size and number of triangles present and on their arrangement. Hence, it is reasonable to state that as the fractal iteration is varied, the antenna impedance will change and the resonant wavelength will shift. The remainder of this investigation is devoted to understanding this phenomenon.

3. Simulation technique and results

Due to its versatility and widespread application, a three-dimensional finite-difference time-domain program is used to simulate the SFPAs. In each simulation, the antenna of interest is placed on a silica substrate with a refractive index $n_s = 1.5$. The antennas are given the properties of gold and the Drude model is used to represent the permittivity function of gold over a wide spectral range. Drude parameters of $\varepsilon_\infty = 9.069$, $\tau_c = 8.669$ fs, and $\omega_p = 1.354 \times 10^{16}$ rad/s are based on an optimal fit to well-established experimental data and ensure that the optical properties of gold are well-represented for the wavelengths of interest [18,19]. The minimum feature size of gold is maintained at or above dimensions of experimentally-confirmed structures for this model [20]. In order to obtain broadband characteristics of the antennas in a single simulation, each antenna is excited by a plane wave that has been temporally modulated by a Gaussian function, permitting access to wavelengths in the range $600\text{nm} \le \lambda \le 4.0\mu\text{m}$. The antennas are excited from below the silica substrate and the electric fields are measured 3nm above the top surface of the antenna. The antenna gap is held

#143637 - $15.00 USD Received 14 Mar 2011; revised 28 Mar 2011; accepted 29 Mar 2011; published 12 May 2011

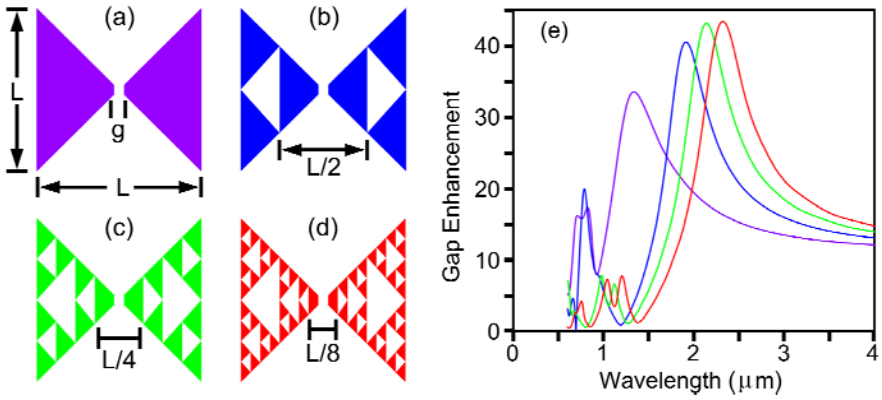

Fig. 1. Schematic representations of the simulations geometries: (a) bowtie antenna and (b) first-, (c) second- and (d) third-iteration Sierpiński fractal plasmonic antennas. The broadband electric field enhancement factor is shown in (e). The antenna color in (a)-(d) corresponds to the line color in (e).

constant at 30nm × 30nm for each structure and the gold film thickness is chosen to be 35nm. A spatial resolution of $\Delta x = \Delta y = \Delta z = 3$nm is used to ensure that the electromagnetic fields in the antenna gap are accurately resolved. A time step of $\Delta t = 4.75$as ensures stability at this resolution. Each triangle is connected to its neighbors by a thin strip to avoid geometric singularities, which also ensures excitation of a collective response from the entire structure (i.e. the triangles are all connected). The flare angle of the antenna is held constant at 90°, so that the length and width of the antenna are equal.

The broad band electric field enhancement factor of each antenna iteration with a constant length, $L = 475$nm, is shown in Fig. 1(e). There are several observations that may be drawn from these spectral response plots. As the iteration of SFPA increases from zero to three, the wavelength of the main resonance is red-shifted from 1.40μm to 2.44μm and the enhancement factor increases from 37 to 49. In addition, there is a rearrangement of the minor resonances that occur at shorter wavelengths. As shown in Fig. 1(e), the bowtie antenna has a minor resonance at $\lambda = 822$nm, whereas the first iteration SFPA has minor resonances at $\lambda = \{660, 787\}$ nm. It should be pointed out that these resonances are much weaker than the main resonance and do not effectively confine incident radiation to the gap. Therefore only the main resonance will be discussed in the remainder of this paper.

In the interest of developing empirical design rules describing the operation of these antennas, the resonant wavelength and resonant enhancement factor have been plotted versus antenna length for the four fractal structures under consideration in Fig. 2 (violet, blue, red, and green curves). From these plots, it is evident that the resonant wavelength scales linearly with the antenna length and that increasing the Sierpiński fractal iteration red-shifts the resonance regardless of the antenna length. One remarkable observation that can be drawn from these plots is that the factor by which the resonant wavelength of the first-iteration antenna is red-shifted when compared to a bowtie antenna of the same length is virtually constant and is approximately 1.41. A similar observation can be made for the second- and third-iteration structures, which are red-shifted by factors of 1.57 and 1.68, respectively, relative to a bowtie antenna of the same length.

In order to verify that fields are confined to the antenna gap and not at other locations of the antenna, the intensity distribution at resonance is calculated for each antenna structure and is shown in Fig. 3. For each SFPA iteration, the incident radiation is confined to the antenna gap and transmission through other triangular holes in the antenna is negligible. The full-width half-maximum is calculated along the vertical direction at the center of each antenna

#143637 - $15.00 USD Received 14 Mar 2011; revised 28 Mar 2011; accepted 29 Mar 2011; published 12 May 2011

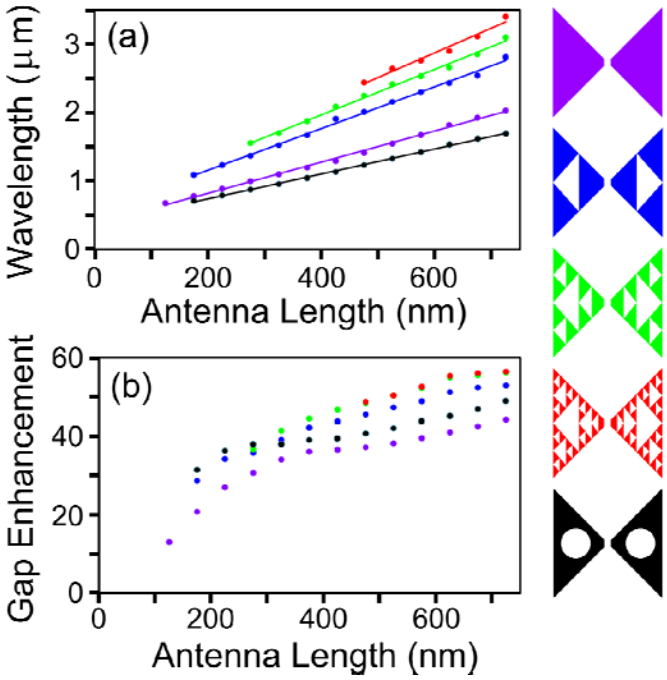

Fig. 2. Empirical relationships between antenna length and (a) resonant wavelength and (b) resonant enhancement factor for each antenna geometry under consideration. The color of antennas on the right corresponds to the line colors in (a) and (b).

gap and is found to be 37.86nm, 37.95nm, 37.90nm, and 37.86nm for the bowtie, first, second, and third iteration antennas with a constant length of 475nm, respectively. Remarkably, as the fractal iteration increases, the resonant wavelength of the antenna is red-shifted, yet allows for confinement to the same nanoscale dimensions. In the case of the bowtie antenna with L = 475nm, incident fields are confined to λ/47 and enhanced by a factor of 37. In comparison, the third iteration SFPA confines incident fields to λ/80 and enhances them by a factor of 49.

4. Geometric investigation

As alluded to earlier, changing the geometry of the antenna changes its ability to polarize, which in turn shifts its resonant wavelength. In an effort to understand the source of the observed red-shift, it is natural to examine the antenna geometry. Table 1 summarizes some of the key geometric properties of each antenna. As the iteration increases, the total volume of gold in the antenna decreases and the total perimeter of the gold features increases. Besides these simple geometric parameters, it is important to consider the possibility that it is the self-similar arrangement of triangles and their ability to polarize that may be the cause of this behavior. In order to understand the importance of each of these parameters (perimeter, area and polarizability), a subsequent series of simulations was performed. A non-fractal test-case was designed to compare with the first iteration antenna. Rather than removing a triangle from the bowtie antenna, a circle with the same area as the triangle was removed. The geometric properties of this structure are shown in Table 1. Several lengths of this structure were simulated, and plots of the resonant wavelength and enhancement factor versus antenna length are shown in Fig. 2, along with the previous results for comparison. Interestingly, the circular structure consistently produces a blue-shifted resonance when compared to the bowtie antenna. The resonant enhancement factor is typically 10% less than for the first iteration SFPA. Even though the area and perimeter properties of the circular structure are comparable

#143637 - $15.00 USD Received 14 Mar 2011; revised 28 Mar 2011; accepted 29 Mar 2011; published 12 May 2011

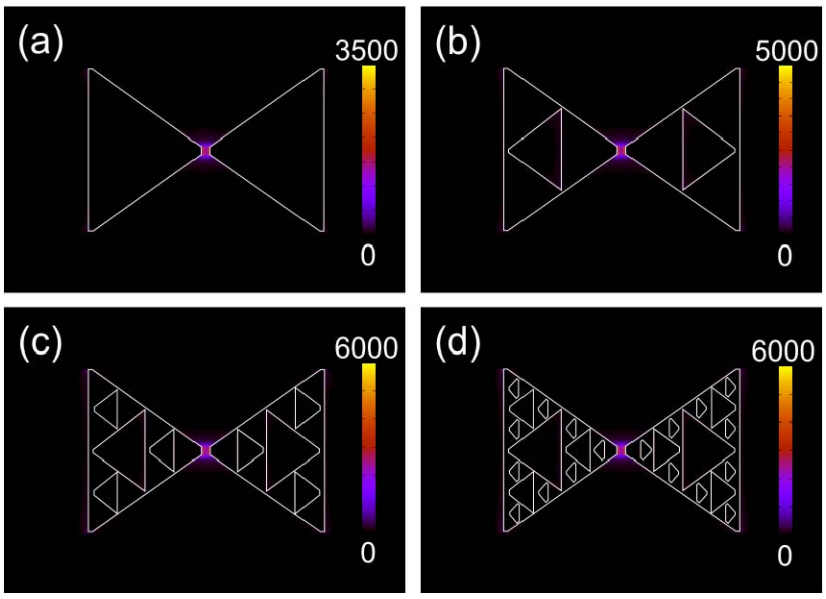

Fig. 3. Intensity distributions at resonance for (a) bowtie antenna and (b) first-, (c) second- and (d) third-iteration Sierpiński fractal plasmonic antennas.

to the fractal structure, the performance is inferior, demonstrating the unique ability of the fractal geometry to produce red-shifted resonances and large confinement factors.

5. Conclusion

The above results provide theoretical insight into the operation of plasmonic bowtie antennas which are modified to contain Sierpiński triangle fractals. We have simulated structures that offer a compact antenna footprint, a large confinement factor, tunability in the range 700nm ≤ λ ≤ 3.4μm and electric field enhancement factors of up to 56 in the center of the antenna gap. Moreover, we have demonstrated that this behavior is related to the ability of the fractal geometry to become polarized. We anticipate that these results will act as a starting point for both theoretical and experimental investigations into plasmonic antennas with fractal or other complex geometries. In addition, these results will contribute to future experiments demonstrating sensitive observation of vibrational modes with a compact device footprint.

Table 1. Geometric Properties of Antennas under Investigation

Antenna	Gold Area	Gold Perimeter	Red-shift Factor
Bowtie	A	P	1.00
First	0.750 × A	1.50 × P	1.41
Second	0.563 × A	2.25 × P	1.57
Third	0.422 × A	3.38 × P	1.68
Circle	0.750 × A	1.37 × P	0.87

Acknowledgements

This work was supported by the Natural Sciences and Engineering Research Council of Canada, Alberta Innovates, and the Canadian Research Chairs Program.

#143637 - $15.00 USD Received 14 Mar 2011; revised 28 Mar 2011; accepted 29 Mar 2011; published 12 May 2011